

San Jose State University

From the Selected Works of Aaron J. Romanowsky

2016

Stellar Populations across the Black Hole Mass–Velocity Dispersion Relation

Ignacio Martín-Navarro, *University of California Observatories*

Jean P. Brodie, *University of California Observatories*

Remco C.E. van den Bosch, *Max Planck Institute for Astronomy*

Aaron J. Romanowsky, *San Jose State University*

Duncan A. Forbes, *Swinburne University of Technology*



Available at: https://works.bepress.com/aaron_romanowsky/118/



STELLAR POPULATIONS ACROSS THE BLACK HOLE MASS–VELOCITY DISPERSION RELATION

IGNACIO MARTÍN-NAVARRO¹, JEAN P. BRODIE¹, REMCO C. E. VAN DEN BOSCH²,
AARON J. ROMANOWSKY^{1,3}, AND DUNCAN A. FORBES⁴

¹ University of California Observatories, 1156 High Street, Santa Cruz, CA 95064, USA; imartin@ucsc.edu

² Max-Planck Institut für Astronomie, Königstuhl 17, D-69117 Heidelberg, Germany

³ Department of Physics and Astronomy, San José State University, 1 Washington Square, San Jose, CA 95192, USA

⁴ Centre for Astrophysics and Supercomputing, Swinburne University, Hawthorn, VIC 3122, Australia

Received 2016 August 29; revised 2016 September 16; accepted 2016 September 19; published 2016 November 14

ABSTRACT

Coevolution between supermassive black holes (BH) and their host galaxies is universally adopted in models for galaxy formation. In the absence of feedback from active galactic nuclei (AGNs), simulated massive galaxies keep forming stars in the local universe. From an observational point of view, however, such coevolution remains unclear. We present a stellar population analysis of galaxies with direct BH mass measurements and the BH mass– σ relation as a working framework. We find that over-massive BH galaxies, i.e., galaxies lying above the best-fitting BH mass– σ line, tend to be older and more α -element-enhanced than under-massive BH galaxies. The scatter in the BH mass– σ – $[\alpha/\text{Fe}]$ plane is significantly lower than that in the standard BH mass– σ relation. We interpret this trend as an imprint of AGN feedback on the star formation histories of massive galaxies.

Key words: galaxies: active – galaxies: evolution – galaxies: formation – galaxies: fundamental parameters – galaxies: general – galaxies: stellar content

1. INTRODUCTION

The suppression of star formation via active galactic nucleus (AGN) feedback plays a crucial role in state-of-the-art numerical simulations (Vogelsberger et al. 2014; Schaye et al. 2015), but its observational effects are difficult to establish. The distribution of AGNs in the color–magnitude plane (Martin et al. 2007; Schawinski et al. 2007) has been traditionally used as an indirect method to empirically constrain any AGN effect in nearby galaxies. With a detailed chemical evolution treatment in the most recent cosmological simulations (e.g., Crain et al. 2015), a new window of opportunity opens for understanding the effect of AGNs on nearby objects. Based on the Evolution and Assembly of GaLaxies and their Environments cosmological simulations, Segers et al. (2016) recently linked AGN feedback to the overabundance of α -elements in massive galaxies—a well-known property of nearby early-type galaxies (Thomas et al. 2005; de La Rosa et al. 2011; Conroy et al. 2014).

The existence of an $[\alpha/\text{Fe}]$ –galaxy mass relation suggests a link between the star formation timescale of a galaxy and its mass. Whereas α -elements are produced in core-collapse supernovae (SNe) with very short lifetimes, the onset of SNe Ia occurs later (~ 1 Gyr), mainly releasing iron to the interstellar medium. Therefore the relative abundance of α -elements to iron reflects how long SNe Ia have been able to pollute the medium: the less α -enhanced a stellar population is, the more extended its star formation. In the scenario proposed by Segers et al. (2016), more massive galaxies host and fuel more massive black holes (BHs) in their centers, leading to a stronger AGN effect that ultimately quenches the star formation more rapidly. The $[\alpha/\text{Fe}]$ –galaxy mass relation would therefore appear as a natural consequence of the coevolution between BHs and galaxies.

However, the (level of) coevolution is still under debate. The BH masses do correlate with the host galaxies properties (see Kormendy & Ho 2013 for a review). The tightest correlation is

the so-called M – σ relation which links the BH mass and stellar velocity dispersion (σ) of the host galaxy (Beifiori et al. 2012; van den Bosch 2016). Whether this BH mass– σ relation results from a causal connection (e.g., Silk & Rees 1998; Fabian 1999; King 2003) or not (Peng 2007; Jahnke & Macciò 2011) remains an open question.

The effect of the AGN feedback depends strongly on the BH accretion rate. Close to the Eddington limit, the amount of energy radiated around the BH is expected to be large enough to effectively quench the ongoing star formation (Fabian 2012). This so-called quasar mode would take place at high redshifts ($z \sim 2$ – 3), and precedes the less energetic maintenance mode, which happens at lower BH accretion rates. The maintenance mode is thought to be responsible for continuously heating the gaseous halos around nearby massive galaxies. The properties of present-day massive galaxies would then be a combination of the early quenching associated with the quasar mode, and the more extended maintenance mode that inhibits further star formation (Choi et al. 2015; Voit et al. 2015).

However, observational evidence of AGN feedback is inconclusive. On the one hand, strong nuclear outflows have been reported in a wide variety of environments, from luminous quasars (Greene et al. 2011) to nearby quiescent galaxies (Cheung et al. 2016). Moreover, Beifiori et al. (2012) have tentatively explored the connection between nuclear activity and the M – σ relation. On the other hand, and contrary to what would be expected from negative AGN feedback, the most (X-ray) luminous AGNs are found in strongly star-forming galaxies (Rovilos et al. 2012).

In this Letter we report our attempts to quantify the effect of the central BH on the evolution of the host galaxy. We conduct a stellar population analysis of galaxies with known BH masses, finding significant differences in the stellar population properties depending on the location of the galaxy in the BH mass– σ plane. This suggests a strong degree of coevolution between galaxies and their central BHs.

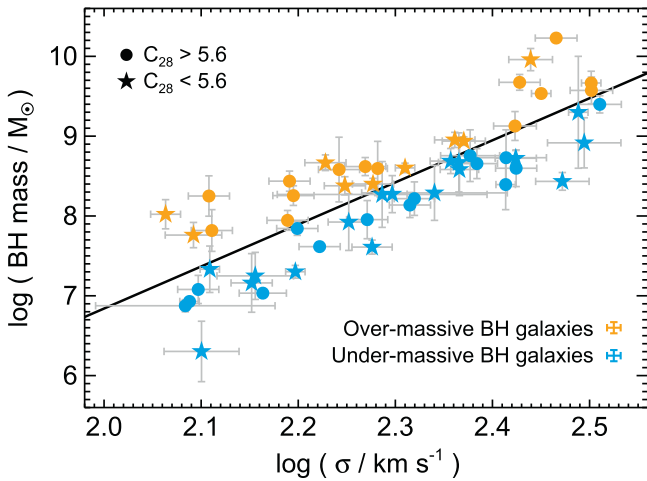


Figure 1. The BH mass–velocity dispersion relation for our sample of galaxies. Orange and blue dots correspond to over-massive and under-massive BH galaxies, i.e., galaxies above and below the best-fitting relation of van den Bosch (2016; black solid line). Objects with highly concentrated brightness profiles ($C_{28} > 5.6$) are shown as filled circles, whereas filled stars correspond to a lower ($C_{28} < 5.6$) concentration index.

2. BH DATA

We use as a reference the BH sample of van den Bosch (2016), which provides not only a large (230 objects) and updated compilation of BH masses and σ , but also consistent measurements of the light profile concentration $C_{28} \equiv 5 \log R_{20}/R_{80}$. The stellar population properties were extracted for galaxies belonging to the Hobby–Eberly Telescope Massive Galaxy Survey (HETMGS, van den Bosch et al. 2015). HETMGS consists of a long-slit spectroscopic survey of 1022 objects, using the Marcario Low Resolution Spectrograph on the 10 m HET, at intermediate spectral resolution (4.8 and 7.5 Å) depending on the slit width (1'' and 2'', respectively). Each object in the sample was observed for at least 15 minutes, covering a spectral range from 4300 to 7400 Å.

After visual inspection, we removed from the sample those objects with poor kinematical fits (signal-to-noise < 5 –10), and also those galaxies where the strength of the emission lines dominated the central spectrum (Amplitude-over-noise > 50), thereby avoiding strong contamination of the Balmer absorption lines, our main age indicator. Finally, we also excluded from the analysis galaxies with recession velocities $z > 0.033$, since prominent telluric lines could affect our stellar population analysis. Although galaxies with velocity dispersions down to $\log \sigma = 1.8$ (km s^{-1}) fulfilled all these criteria, the vast majority of objects ranged from $\log \sigma = 2$ to $\log \sigma = 2.5$. Moreover, for galaxies below the L^* characteristic luminosity, the star formation efficiency is mainly regulated by stellar feedback (Silk & Mamon 2012). Thus, to isolate the effect of the AGNs in our sample, we limited our study to galaxies with $\log \sigma > 2$.

Our working sample consists of 57 galaxies, with BH mass, σ , and R_c measurements, plus long-slit spectroscopic data to perform the stellar population analysis. Figure 1 shows the BH mass– σ relation for the sample, where different symbols indicate different concentration indices. The threshold value $C_{28} = 5.6$ corresponds to the median of the distribution.

3. STELLAR POPULATION ANALYSIS

The stellar population analysis is based on the latest version of the MILES models (Vazdekis et al. 2010, 2015), which

range from 0.03 to 14 Gyr in age, from -2.27 to $+0.40$ dex in metallicity, and from $+0.0$ to $+0.4$ dex in $[\alpha/\text{Fe}]$. The slope of the stellar IMF was assumed to have the Milky Way value ($\Gamma_b = 1.3$ in the MILES notation; Kroupa 2002). All our measurements are luminosity-weighted, single stellar population equivalent values.

To perform a homogeneous stellar population analysis we extracted the central spectrum of each galaxy within a fixed aperture of $R_c/8$. We then used the Penalized Pixel-fitting code (Cappellari & Emsellem 2004) to simultaneously fit the kinematics and remove the nebular emission.

Although the information in line-strength indices is mainly encoded in the depth of the spectral features, index measurements are also sensitive to the shape of the continuum. Therefore, before attempting a detailed line-strength analysis, the HETMGS data must be flux-calibrated. To do so, we first obtain a zero-order estimate of the stellar population parameters by fitting the prominent $\text{H}\beta$, $\text{Mgb}5170$, $\text{Fe}5270$, and $\text{Fe}5335$ lines after removing their continuum. This leads to approximate age, metallicity, and $[\text{Mg}/\text{Fe}]$ values, which are used to estimate a best-fitting template. We then divide the observed spectrum by the best-fitting template, fitting this ratio by a low (4th grade) order polynomial that is finally used to correct the continuum. Our entire analysis is based on these continuum-corrected spectra.

To derive the abundance ratios we follow the approach described in (Vazdekis et al. 2015, Section 8.2.4), which consists of two basic steps. First, the mean (luminosity-weighted) age is measured using a standard $\text{H}\beta$ – $[\text{MgFe}]'$ diagram.⁵ Second, the $[\text{Mg}/\text{Fe}]$ value is calculated as the difference between the Mg and Fe metallicities, corrected by a constant factor. More explicitly, our $[\text{Mg}/\text{Fe}]$ ratio is given by

$$[\text{Mg}/\text{Fe}] = C \times ([\text{M}/\text{H}]_{\text{Mgb}} - [\text{M}/\text{H}]_{\langle\text{Fe}\rangle}), \quad (1)$$

where $[\text{M}/\text{H}]_{\text{Mgb}}$ and $[\text{M}/\text{H}]_{\langle\text{Fe}\rangle}$ are the best-fitting metallicities measured at fixed age, measured from the Mgb and $\langle\text{Fe}\rangle$ line-strength indices, respectively. The constant factor, C , depends on the set of models; for the MILES solar scale models, based on the BaSTI set of isochrones (Pietrinferni et al. 2004, 2006), it has a value of 0.59 (Vazdekis et al. 2015).

In summary, we used the $\text{H}\beta$ and $[\text{MgFe}]'$ line-strength indices to constrain ages and metallicities, and we assume $[\text{Mg}/\text{Fe}]$ to be a proxy for the $[\alpha\text{-elements}/\text{Fe}]$ ratio. The relative nature of this method for deriving the abundance ratio might not perfectly capture the absolute $[\text{Mg}/\text{Fe}]$ value, but it is well-suited for a relative comparison, as intended in this Letter, since it minimizes the sensitivity of our results to unavoidable degeneracies.

4. RESULTS

To investigate the influence of the BH on the stellar population properties of the host galaxies, we divide our sample into over-massive BH galaxies (i.e., galaxies lying above the BH mass– σ relation) and under-massive BH galaxies (Figure 1), using the best-fitting relation derived in van den Bosch (2016).

In the local universe, the stellar population properties of galaxies correlate with their central σ (e.g., Peletier 1989; Thomas et al. 2005; La Barbera et al. 2013), which is generally interpreted as a galaxy-mass-driven evolution. In order to

⁵ We used the $\text{H}\beta$ and $[\text{MgFe}]'$ indices as defined in Cervantes & Vazdekis (2009) and Thomas et al. (2003), respectively.

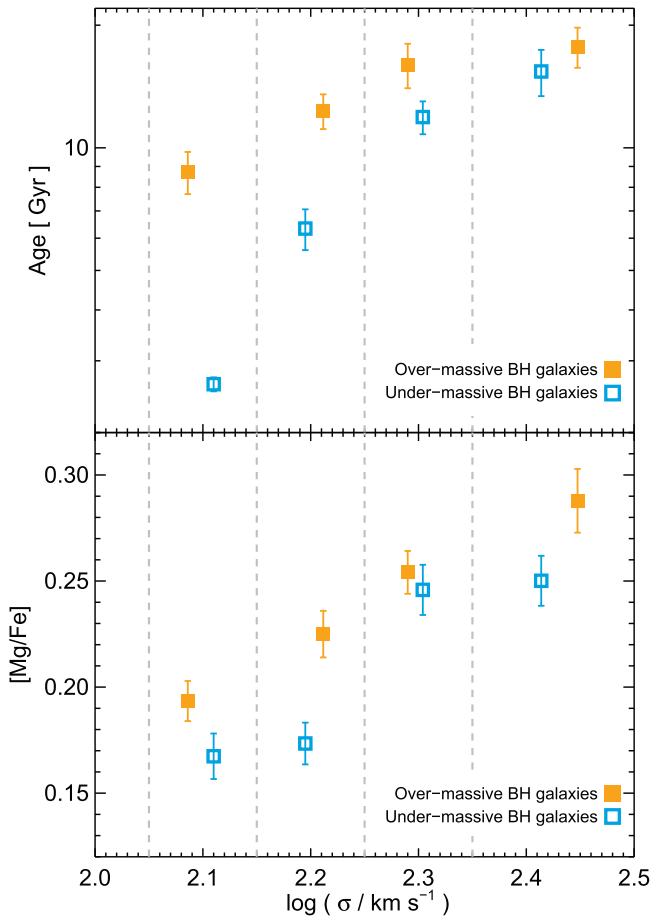


Figure 2. Age (top) and $[Mg/Fe]$ (bottom) variations as a function of galaxy velocity dispersion for over-massive (orange) and under-massive (blue) BH galaxies. The dashed vertical lines indicate the different σ bins, and measurements come from our stacked spectra. Two main trends are shown in this figure. First, as expected, the age and the $[Mg/Fe]$ ratio increase with σ . Second, the stellar population properties depend on the central BH mass, being older and more α -enhanced for galaxies that host a more massive BH at fixed σ .

remove these trends from the analysis, we study the variations in stellar population properties at fixed σ , dividing our sample of galaxies into four bins. For each of these bins we stack the spectra of over-massive and under-massive BH galaxies, and we calculate their (averaged) stellar population properties.

Figure 2 shows the best-fitting age and $[Mg/Fe]$ values in our four σ bins, for over-massive and under-massive BH galaxies. In general, galaxies become older and more α -enhanced with increasing σ . The fact that we recover the expected trends with galaxy mass reinforces the consistency of our stellar population analysis. In addition to this well-known dependence with σ , we observe a clear difference depending on the mass of the BH: galaxies that have more massive BHs at fixed σ also tend to be older and more α -enhanced.

The decreasing age difference with increasing galaxy mass can be understood as a combination of two factors. First, line-strength analysis provides luminosity-weighted values, with ages being more sensitive to this bias than they are to metallicity and α -enhancement (Serra & Trager 2007). Thus, although the relative differences in age might be similar along the whole sample, they appear more prominent when probing lower-mass and therefore younger galaxies. Note that a small fraction of young stars could boost these luminosity-weighted

Table 1
Best-fitting Ages and $[Mg/Fe]$ Ratios

Galaxy	Age (Gyr)	$[Mg/Fe]$ (dex)	Galaxy	Age (Gyr)	$[Mg/Fe]$ (dex)
NGC 0307	13.2	0.18	NGC 3842	16.0	0.31
NGC 0315	19.7	0.17	NGC 3953	7.0	0.10
NGC 0383	17.5	0.20	NGC 4026	14.9	0.13
NGC 0524	12.2	0.21	NGC 4143	17.0	0.20
NGC 0541	16.7	0.19	NGC 4203	19.7	0.14
NGC 0741	17.8	0.21	NGC 4261	12.6	0.21
NGC 0821	10.1	0.16	NGC 4335	8.9	0.17
NGC 1023	16.8	0.18	NGC 4350	9.7	0.18
NGC 1271	19.5	0.23	NGC 4459	3.0	0.14
NGC 1277	18.6	0.32	NGC 4473	11.6	0.18
NGC 1961	5.5	0.15	NGC 4564	8.9	0.20
NGC 2892	12.6	0.19	NGC 4649	15.7	0.33
NGC 2960	1.4	0.00	NGC 4698	16.4	0.18
NGC 3115	8.3	0.22	NGC 5127	11.3	0.20
NGC 3245	11.2	0.15	NGC 5490	16.0	0.24
NGC 3368	2.07	0.06	NGC 5576	3.6	0.12
NGC 3377	9.8	0.24	NGC 6086	19.4	0.25
NGC 3379	17.5	0.24	NGC 7052	14.4	0.20
NGC 3414	15.7	0.19	NGC 7331	2.6	0.20
NGC 3607	8.0	0.20	NGC 7619	7.4	0.29
NGC 3608	14.7	0.22	NGC 7768	18.9	0.27
NGC 3627	1.3	0.10	MRK 1216	19.6	0.24

Note. Here we only include galaxies where the signal-to-noise allowed a reliable stellar population analysis. Ages older than 14 Gyr are due to very low $H\beta$ values and the fact that we assumed a universal IMF slope (La Barbera et al. 2013).

measurements, which therefore should be considered as upper limits for the age difference. Second, as the stellar populations get older, our precision in the age determination decreases. Consequently, as we consider the massive end of our sample, the ages of the galaxies tend to be indistinguishable.

Differences in the $[Mg/Fe]$ ratio are less dependent on σ . Note that for low-mass galaxies, the $[Mg/Fe]$ ratio is also biased toward young stellar populations, which by definition result from more extended star formation histories and therefore are less α -enhanced. The $\sigma \sim 2.3 \log \text{km s}^{-1}$ bin shows a similar $[Mg/Fe]$ value for under-massive and over-massive BH galaxies. We suggest that this is due to a small range in the BH masses for that particular bin (~ 0.5 dex, compared to a typical ~ 1 dex for the other bins), which is apparent in Figure 1.

As an additional test we compare individual BH masses and stellar population measurements, which are listed in Table 1. As stated above, both BH masses and stellar population properties correlate with σ , so this galaxy-mass dependency has to be corrected to isolate the potential BH effect. In Figure 3, we show the residuals in the BH mass– σ relation plotted against the residuals of the $[Mg/Fe]$ – σ relation, for individual galaxies. After removing the main correlation with σ , those galaxies hosting more massive BHs also exhibit more α -enhanced stellar populations. Note that Figure 3 shows measurements over a wide range of $\log \sigma$ (2.0–2.5), further supporting the averaged trend shown in Figure 2. Two clear outliers depart from the global trend. In the upper left corner of Figure 2 NGC 2787 has a pseudo-bulge with an enhanced $[Mg/Fe]$ ratio (+0.26 dex) and a relatively low-mass BH ($10^{7.6} M_{\odot}$), pointing toward a non-AGN-related quenching process. More interesting is the other outlier, NGC 1600, a

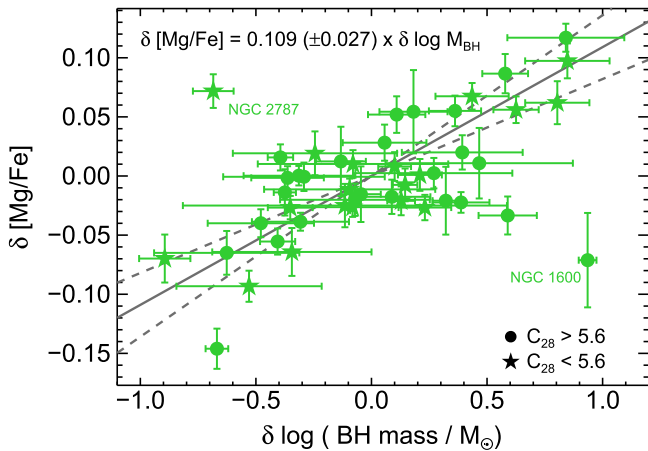


Figure 3. [Mg/Fe] vs. BH mass for individual galaxies. The residuals from the [Mg/Fe]– σ relation correlate positively with the scatter in the BH mass– σ relation. The solid line corresponds to the best-fitting relation, and the dashed lines indicate the uncertainty in the fit. At a given σ , the α -enhancement of a galaxy seems to follow the mass of its central BH. Filled circles and stars indicate high and low concentration indices, respectively.

galaxy with a very massive BH but that shows a relatively mild α enhancement. Either the [Mg/Fe] or the BH mass measurements of NGC 1600 are incorrect, or the present-day BH mass was reached after the bulk of the star formation took place in the host galaxy.

Finally, in Figure 4 we make use of the correlation, at fixed σ , between BH mass and [Mg/Fe], to revisit the fundamental BH mass– σ relation. Although σ is known to be the main and almost only relevant parameter for determining the BH mass (Beifiori et al. 2012; van den Bosch 2016), we found that also taking into account the [Mg/Fe] values significantly reduces the scatter, from $\epsilon = 0.41 \pm 0.06$ to $\epsilon = 0.26 \pm 0.04$. To be consistent with the analysis presented in van den Bosch (2016), we used the Bayesian routines of Kelly (2007) to estimate both the scatter and the best-fitting relations shown in Figure 4.

5. DISCUSSION AND CONCLUSIONS

Understanding the mechanism responsible for quenching the star formation within massive galaxies is a difficult task. In the local universe, a detailed analysis of their stellar populations is possible, but quenching is no longer taking place. At higher redshifts ($z \gtrsim 2-3$), where massive galaxies ceased forming new generations of stars, obtaining sufficiently good spectra is out of reach for the current generation of telescopes.

In this Letter we made use of two observables left behind in the natural evolution of galaxies: the BH as a power source of the AGN activity, and the abundance pattern of stars as a proxy for the formation timescale of the stellar populations. Our findings, summarized in Figures 2 and 3, indicate a strong connection between the stellar population properties of a galaxy and the mass of its central BH. In particular, stars within over-massive BH galaxies tend to be older and more α -enhanced, suggesting a more rapid quenching process than that in under-massive BH galaxies.

It could be argued that our findings result from spurious correlations with unrecognized parameters. However, Beifiori et al. (2012) and van den Bosch (2016) have shown that the residuals of the BH mass– σ relation do not correlate with structural parameters of galaxies.

An alternative scenario could involve a sample biased toward later-type galaxies below the BH mass– σ relation (Kormendy et al. 2011). Nevertheless, we rule out this possibility because the observed trend also extends to the most massive galaxies in our sample, where only early-type galaxies are found. In addition, after removing the pseudo-bulges from the analysis, the same trends with BH mass are recovered. Greene et al. (2016) recently claimed that megamaser disk galaxies are slightly offset from the main BH mass– σ relation. Most of these objects were removed because their spectra displayed strong nebular emission within the H_β line, and only one megamaser (NGC 2960) is present in the final sample. As expected from our findings, and given its relatively low BH mass, NGC 2960 shows almost no α -enhancement ([Mg/Fe] = 0.003).

Note that, although not ideal, our approach for correcting the stellar continuum does not introduce any bias into our stellar population analysis, since it is completely independent of the mass of the BH. In principle, the mass of the BH in α -enhanced galaxies could be overestimated if a solar-scaled ([Mg/Fe] = 0) mass-to-light ratio (M/L) is assumed. However, the effect of the abundance pattern on the M/L is very mild, and is only significant for filters bluer than $\lambda_{\text{eff}} \sim 4000 \text{ \AA}$ (Vazdekis et al. 2015). Moreover, since dynamical models commonly assume a radially constant M/L , a pronounced gradient may also affect the BH measurement. In this regard, Sánchez-Blázquez et al. (2007) have shown that more massive and α -enhanced ETGs galaxies have flatter gradients in their stellar population properties, and thus, more constant M/L profiles (Martín-Navarro et al. 2015). Thus, we do not expect a systematic bias in the BH masses, due to the stellar population properties of the host galaxies.

We interpret our results as a direct connection between the central BH and the star formation history of galaxies. More massive BHs would have formed earlier and in denser regions of the universe, feeding more active AGNs and thus quenching the star formation more quickly. This scenario leads to older and more α -enhanced stellar populations. As the BH mass and the AGN feedback decreased, galaxies would form later, creating stars over more extended periods of time, leading to lower [Mg/Fe] and younger ages. For galaxies above L^* , such as those studied in this work, the effect of stellar feedback, even in the early stages of galaxy formation, is expected to be negligible. However, a natural prediction of this AGN-driven quenching is that the differences between over-massive and under-massive galaxies would start vanishing for objects below L^* .

Does this mean that the chemical enrichment of massive galaxies is entirely determined by the AGN activity in the early universe? The abundance pattern of a galaxy depends on two factors: the formation timescale of its stellar populations and the number of massive stars responsible for the chemical enrichment, i.e., the stellar initial mass function (IMF). Consequently, an enhanced [Mg/Fe] can result from a short star formation event or from a more extended star formation history but with a flat (giant-dominated) IMF (Vazdekis et al. 1996; Thomas et al. 1999). While our analysis at fixed σ shows an enhanced [Mg/Fe] for over-massive BH galaxies, therefore supporting a connection between AGNs and the abundance pattern, the IMF might also be playing an important role in establishing the [Mg/Fe]– σ relation. In particular, it has been shown that a time-varying IMF, which is flatter at earlier epochs, is necessary to reconcile the chemical properties of

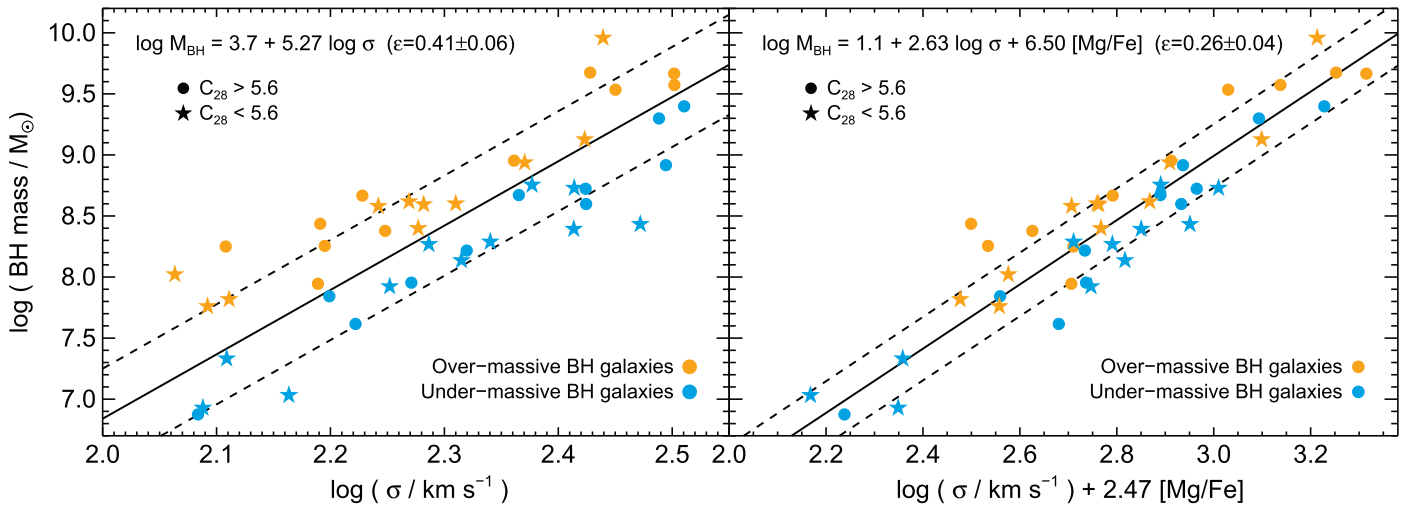


Figure 4. Best-fitting relations between observed BH masses, velocity dispersion, and [Mg/Fe]. The solid line corresponds to the best-fitting solution, and the dashed lines indicate the intrinsic scatter. The orange and blue symbols indicate over-massive and under-massive BH galaxies, and filled circles and stars indicate high and low concentration indices, respectively. The left panel shows the reference BH mass– σ relation, whereas in the right panel we fitted a regression of the form $\log M_{\text{BH}} = \text{constant} + \alpha \log \sigma + \beta[\text{Mg}/\text{Fe}]$, which has a significantly lower scatter. Neither of the two panels includes the two outliers of Figure 3.

nearby massive galaxies and their apparently non-universal IMF (Weidner et al. 2013; Ferreras et al. 2015; Martín-Navarro 2016). Numerical simulations have also supported the idea of a flat IMF during the early formation of massive galaxies (Calura & Menci 2009; Arrigoni et al. 2010; Fontanot et al. 2016). Thus, the [Mg/Fe]– σ relation is potentially driven by a combination of the two processes, AGN-related quenching plus a non-universal IMF.

Irrespective of the origin of the abundance pattern in galaxies, our results demonstrate, observationally, a strong correlation between black hole masses and the star formation histories of galaxies, which we interpret as AGN feedback directly driving the star formation history of massive galaxies.

We acknowledge support from NSF grants AST-1211995 and AYA2013-48226-C3-1-P from the Spanish Ministry of Economy and Competitiveness (MINECO). We would like to thank the anonymous referee for constructive comments that improved the original manuscript. I.M.N. would like to thank Jesús Falcón-Barroso, Luis Peralta de Arriba, and Marja Seidel for their useful comments and suggestions.

REFERENCES

- Arrigoni, M., Trager, S. C., Somerville, R. S., & Gibson, B. K. 2010, *MNRAS*, **402**, 173
- Beifiori, A., Courteau, S., Corsini, E. M., & Zhu, Y. 2012, *MNRAS*, **419**, 2497
- Calura, F., & Menci, N. 2009, *MNRAS*, **400**, 1347
- Cappellari, M., & Emsellem, E. 2004, *PASP*, **116**, 138
- Cervantes, J. L., & Vazdekis, A. 2009, *MNRAS*, **392**, 691
- Cheung, E., Bundy, K., Cappellari, M., et al. 2016, *Natur*, **533**, 504
- Choi, E., Ostriker, J. P., Naab, T., Oser, L., & Moster, B. P. 2015, *MNRAS*, **449**, 4105
- Conroy, C., Graves, G. J., & van Dokkum, P. G. 2014, *ApJ*, **780**, 33
- Crain, R. A., Schaye, J., Bower, R. G., et al. 2015, *MNRAS*, **450**, 1937
- de La Rosa, I. G., La Barbera, F., Ferreras, I., & de Carvalho, R. R. 2011, *MNRAS*, **418**, L74
- Fabian, A. C. 1999, *MNRAS*, **308**, L39
- Fabian, A. C. 2012, *ARA&A*, **50**, 455
- Ferreras, I., Weidner, C., Vazdekis, A., & La Barbera, F. 2015, *MNRAS*, **448**, L82
- Fontanot, F., De Lucia, G., Hirschmann, M., et al. 2016, *MNRAS*, submitted (arXiv:1606.01908)
- Greene, J. E., Seth, A. C., Kim, M., et al. 2016, *ApJL*, **826**, L32
- Greene, J. E., Zakamska, N. L., Ho, L. C., & Barth, A. J. 2011, *ApJ*, **732**, 9
- Jahnke, K., & Macciò, A. V. 2011, *ApJ*, **734**, 92
- Kelly, B. C. 2007, *ApJ*, **665**, 1489
- King, A. 2003, *ApJL*, **596**, L27
- Kormendy, J., Bender, R., & Cornell, M. E. 2011, *Natur*, **469**, 374
- Kormendy, J., & Ho, L. C. 2013, *ARA&A*, **51**, 511
- Kroupa, P. 2002, *Sci*, **295**, 82
- La Barbera, F., Ferreras, I., Vazdekis, A., et al. 2013, *MNRAS*, **433**, 3017
- Martin, D. C., Wyder, T. K., Schiminovich, D., et al. 2007, *ApJS*, **173**, 342
- Martín-Navarro, I. 2016, *MNRAS*, **456**, L104
- Martín-Navarro, I., La Barbera, F., Vazdekis, A., et al. 2015, *MNRAS*, **451**, 1081
- Peletier, R. F. 1989, PhD thesis, Univ. Groningen
- Peng, C. Y. 2007, *ApJ*, **671**, 1098
- Pietrinferni, A., Cassisi, S., Salaris, M., & Castellì, F. 2004, *ApJ*, **612**, 168
- Pietrinferni, A., Cassisi, S., Salaris, M., & Castellì, F. 2006, *ApJ*, **642**, 797
- Rovilos, E., Comastri, A., Gilli, R., et al. 2012, *A&A*, **546**, A58
- Sánchez-Blázquez, P., Forbes, D. A., Strader, J., Brodie, J., & Proctor, R. 2007, *MNRAS*, **377**, 759
- Schawinski, K., Thomas, D., Sarzi, M., et al. 2007, *MNRAS*, **382**, 1415
- Schaye, J., Crain, R. A., Bower, R. G., et al. 2015, *MNRAS*, **446**, 521
- Segers, M. C., Schaye, J., Bower, R. G., et al. 2016, *MNRAS*, **461**, L102
- Serra, P., & Trager, S. C. 2007, *MNRAS*, **374**, 769
- Silk, J., & Mamon, G. A. 2012, *RAA*, **12**, 917
- Silk, J., & Rees, M. J. 1998, *A&A*, **331**, L1
- Thomas, D., Greggio, L., & Bender, R. 1999, *MNRAS*, **302**, 537
- Thomas, D., Maraston, C., & Bender, R. 2003, *MNRAS*, **339**, 897
- Thomas, D., Maraston, C., Bender, R., & Mendes de Oliveira, C. 2005, *ApJ*, **621**, 673
- van den Bosch, R. 2016, *ApJ*, **831**, 134
- van den Bosch, R. C. E., Gebhardt, K., Gültekin, K., Yıldırım, A., & Walsh, J. L. 2015, *ApJS*, **218**, 10
- Vazdekis, A., Casuso, E., Peletier, R. F., & Beckman, J. E. 1996, *ApJS*, **106**, 307
- Vazdekis, A., Coelho, P., Cassisi, S., et al. 2015, *MNRAS*, **449**, 1177
- Vazdekis, A., Sánchez-Blázquez, P., Falcón-Barroso, J., et al. 2010, *MNRAS*, **404**, 1639
- Vogelsberger, M., Genel, S., Springel, V., et al. 2014, *MNRAS*, **444**, 1518
- Voit, G. M., Donahue, M., Bryan, G. L., & McDonald, M. 2015, *Natur*, **519**, 203
- Weidner, C., Ferreras, I., Vazdekis, A., & La Barbera, F. 2013, *MNRAS*, **435**, 2274